Discriminating lithospheric and asthenospheric anisotropy beneath Northern Oman: sharp contrast observed at the Semail Gap Fault Zone

A. Komeazi[1], A. Kaviani[1], G. Rümpker[1,2], C. Weidle[3], and T. Meier[3]

1. Institute of Geosciences, Goethe-University Frankfurt, Frankfurt, Germany

2. Frankfurt Institute for Advanced Studies, Frankfurt, Germany

3. Institute of Geosciences, Christian-Albrechts-University Kiel, Germany

Corresponding author: Abolfazl Komeazi (komeazi@geophysik.uni-frankfurt.de)

Key Points:

- Depth-dependent anisotropy is observed in the eastern part of Northern Oman.
- A sharp contrast in shear wave splitting parameters is observed at the Semail Gap Fault Zone.
- A change in lithosphere thickness occurs from west to east in Northern Oman

Abstract

To gain a deeper understanding of the extensive and varied lithospheric deformations beneath northern Oman, we examine seismic anisotropy in this region using splitting analysis of teleseismic shear wave data. Our study utilizes data from a dense network consisting of 13 permanent and 45 temporary seismic stations, which were operational for approximately 2.5 years starting from 2013. By examining the azimuthal distribution of shear wave splitting (SWS) parameters, we are able to divide the study area into three sub-regions. The stations located to the west of the Hawasina window exhibit relatively azimuthally invariant SWS parameters suggesting a single anisotropic layer. On the other hand, most of the stations located in the central and eastern regions display a 90-degree periodicity versus back-azimuth, indicating the presence of depth-dependent anisotropy.

The General NW-SE trend of the Fast Polarization Directions (FPDs), one-layer/upper layer FPDs in the east and one-layer FPDs in the west, is concordant with the strike of the structures resulting from the collision between the continental and oceanic plates. Notably, a distinct contrast in the SWS parameters is observed at Semail Gap Fault Zone (SGFZ), suggesting that the SGFZ can be a geological border for the mafic intrusive emplacement from the east. Furthermore, the fast axes of the lower layer exhibit an NE-SW trend, which may be indicative of the large-scale mantle flow resulting from the present-day plate motion.

Keywords: seismic anisotropy, Semail Gap Fault Zone, obduction, northern Oman, shear wave splitting, lithosphere.

Plain Language Summary

In this study, we investigated how the lithosphere beneath northern Oman is deformed by using shear wave splitting (SWS) analysis. We used a dense network of 58 seismic stations, including both permanent and temporary stations. Based on our shear wave splitting observations the region can be divided into three parts. In the west, the splitting parameters (delay time and fast polarization direction) are generally consistent, which is in good agreement with the rigid continental lithosphere, suggesting a single anisotropic layer. In the central and eastern regions, the splitting parameters show different behaviors, indicating more complex and depth-dependent structures. Notably, the Semail Gap Fault Zone (SGFZ) marked a significant boundary in SWS parameters, which represent the SGFZ as a geological boundary. Additionally, NE-SW fast axes indicate large-scale mantle flow due to present-day plate motion.

1 Introduction

The Semail ophiolite in northern Oman is a prime example of obducted oceanic lithosphere and its structure and tectonic evolution have been subject to geoscientific investigations for decades (e.g., Glennie et al., 1974; Searle and Malpas, 1980). Geological studies (e.g., Hacker et al., 1996 a,b; Nicolas et al., 1994, 2000; Searle and Cox, 1999; Rioux et al., 2016; Guilmette et al., 2018; Ambrose and Searle, 2019) shed light on the chronological phases and the background geological setting contributed to the formation of oceanic lithosphere, dynamics of obduction and the development of the north Oman orogeny. This provides a comprehensive understanding of the shallow crustal tectonic evolution of the continent below the ophiolites. However, the significance of pre-obduction tectonic processes in shaping the Arabian continental lithosphere, as well as their role in understanding obduction geometry and dynamics in detail, has been demonstrated only recently (e.g., Weidle et al., 2022, 2023).

Two major tectonic events had left their mark before the obduction of the Semail ophiolite, the Neoproterozoic assembly of Gondwana and the Permo-Triassic breakdown of Pangea. Both these events are reflected in today's lithospheric architecture in northeast Arabia. Previous surface wave tomography studies provided information about the lithospheric thickness and Moho depth of the study region (e.g., Priestley et al., 2012; Pilia et al., 2020a,b, 2021; Weidle et al., 2022; Weidle et al., 2023). Global and regional tomography models (e.g., Al-Lazki et al., 2014; Koulakov et al., 2016; Celli et al., 2020a,b) suggest that mantle lithospheric thickness decreases from > 200 km to ~100 km from the neocratonic core of Arabia towards the margins (Weidle et al., 2023). Furthermore, the crust northwest of the Semail Gap Fault Zone (SGFZ) is typically continental with an average Moho depth of ~40 km, whereas it thins to the east and is likely modified by significant mafic reworking during the mafic breakup of Pangea (Weidle et al., 2023). Given the significant change of crustal architecture across the SGFZ in northern Oman, a main question arises whether similar variations occur in the mantle lithosphere. In the absence of detailed tomographic images of the area, observations from seismic anisotropy could provide more insights into structural properties of the continental lithosphere in the area.

The significance of seismic anisotropy in understanding the deformation and flow pattern in the upper mantle has grown in the last two decades. Seismic anisotropy signatures appear in the mantle and crustal rocks as a result of prolonged deformation and shearing within the mantle and lithosphere (e.g., Savage, 1999; Long and Silver, 2009). In general, the main mechanisms that contribute to seismic anisotropy include Lattice-preferred orientation (LPO) of anisotropic minerals, in particular olivine (Hess, 1964; McKenzie, 1979), caused by flow-induced strain (e.g., Long and Silver, 2009; Savage, 1999), and Shape-preferred orientation (SPO) in the form of fluid-filled cracks in the crust or of aligned mineral aggregates in a deformed lithospheric mantle (e.g., Holtzman and Kendall, 2010). However, anisotropy can also be due to frozen-in lithospheric deformation which has been formed from prior tectonic processes (Barruol et al., 1998; Silver,

1996) in regions where considerable deformation has occurred (e.g., collisional zones, faults and shear zones). Hence, investigating seismic anisotropy can help illuminate the evolution of the lithospheric mantle. Northern Oman is a continental margin that has experienced an extensive developing process of orogeny, rifting and basin formation. There is, therefore, a strong likelihood that seismic anisotropy in the region is caused by "fossil" fabrics preserved in the lithosphere, shearing at the base of the lithospheric plate due to present-day plate motion and local sub-lithospheric mantle convective flow, or a combination of these mechanisms.

Shear-wave splitting of core-refracted phases (e.g., SKS, SKKS, PKS, named XKS henceforth) is one of the most common manifestations of seismic anisotropy (Silver and Chan, 1991). Shear-waves by entering an anisotropic medium exhibit birefringence and split into two separate orthogonal quasi shear-waves which travel at different wave speeds. The delay time, δt, between the fast and slow components and the polarization direction of the fast component (FPD), φ, represent the strength and orientation of seismic anisotropy, respectively.

In the present study, we analyze data from a temporary seismic network consisting of 45 stations completed by 13 permanent stations, which cover the entire region of northern Oman and intersect its major tectonic structures. Shear-wave splitting methods and teleseismic core-refracted phases as input data are employed to infer seismic anisotropy. In this research, we examine how lithospheric deformation and mantle flow are linked to seismic anisotropy, providing more insights into the historical and current status of the lithosphere beneath northern Oman.

2 Geological setting

The study area is located at the northeastern edge of the Arabian plate (Figure 1a), composed of Neoproterozoic island arcs and ophiolites formed during the Pan-African orogeny (Allen et al., 2007; Cozzi et al., 2012). As a result of opening of the Neotethys Ocean, the northern Oman (located in the former Gondwana terrane) experienced rifting and passive margin tectonics (Pillevuit et al., 1997; Ruban et al., 2007) during the Late Carboniferous. This tectonic evolution was followed by the obduction of the Semail Ophiolite in late Cretaceous (e.g., Tippit et al., 1981), and post obduction processes, including late Eocene extension which led to the uplift of Oman mountains (Ninkabou et al., 2021, Weidle et al., 2023).

The subsurface structure beneath the study area has undergone multiple phases of deformation during various geological periods since the Permian breakup of Pangea. Regional-scale tomographic images (e.g., Shad Manaman et al., 2011; Pilia et al., 2020) illustrate a transition from thick to thin crust across the northern Oman from west to east. Pilia et al. (2020) derived higher velocities in the Gulf of Oman and lower velocities towards the west. They attribute this velocity

transition zone to the boundary between the Cretaceous Tethyan oceanic lithosphere and the Arabian passive continental margin. Surface wave tomography investigations (Wiesenberg et al., 2022; Weidle et al., 2022) demonstrate that the Arabian foreland crust, west of the Jabal Akhdar zone, has a thickness of 40–44 km and exhibits seismic properties typical of felsic continental crust. The Vp/Vs ratio in their results depicts a transition from felsic to mafic lithology compositions, which occurs within the area spanning from Jabal Akhdar zone to the SGFZ. Moving eastwards, the Moho depths decrease to 30-35 km, and an increased lower crustal Vs value suggests the presence of mafic intrusions.

Large-scale tomography studies (e.g., Celli et al., 2020a,b) have depicted variations in shear velocity within the lithospheric mantle of the Arabian plate. The cold lithospheric mantle of the ancient Arabian craton meets the low-velocity region beneath northern Oman. Al-Lazki et al. (2014) associated the very low Pn velocity in northern Oman with a hot upper mantle, likely indicating the presence of partial melt beneath this region. Furthermore, Weidle et al. (2023) discuss how this hot material emerges from depths greater than 200 km below Africa-Arabia and rises to approximately 80 km on the northern Oman margins, causing partial remelting and erosion of the lithosphere through small-scale convection at the craton edge.

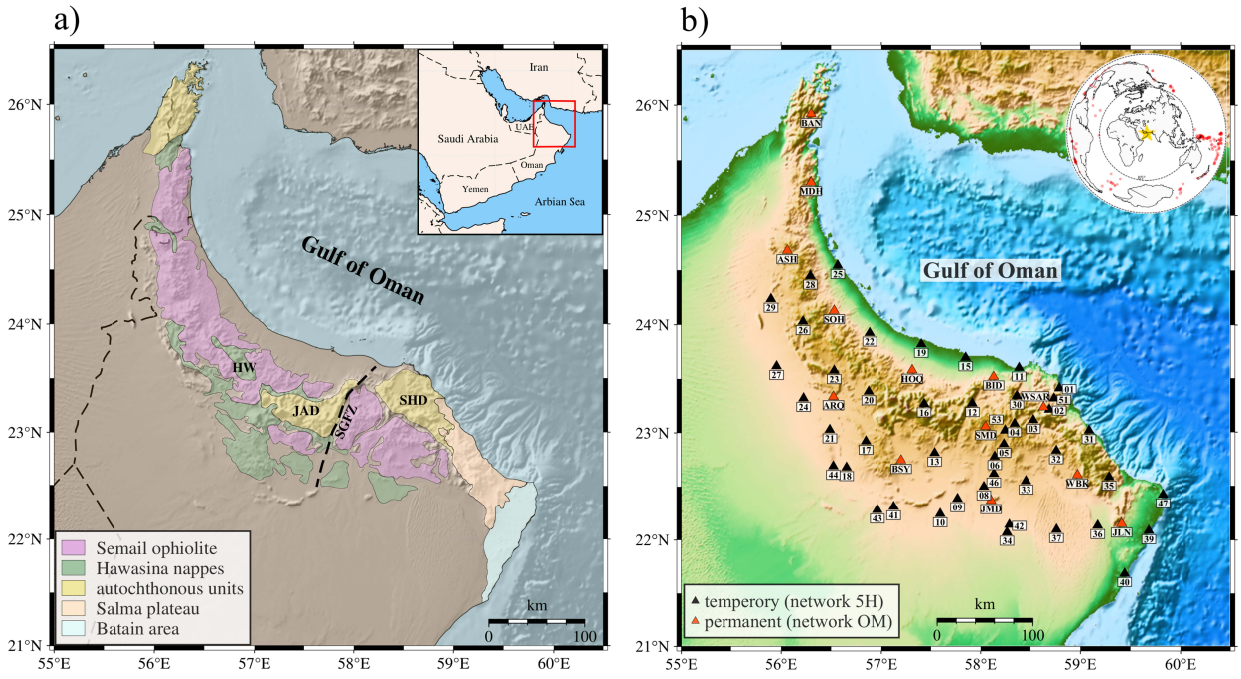

Figure 1. a) An overview map of the tectonic setting in northern Oman (after Scharf et al., 2019). SHD, Saih Hatat dome. JAD, Jabal Akhdar dome. HW, Hawasina Window. SGFZ, Semail Gap Fault Zone, b) Map showing the temporary (black triangles, network 5H) and permanent (red triangles, network OM) seismic stations used in this study. The inset map shows the event distribution within the epicentral distance of 85°-140° used to extract the XKS waveform data.

3 Data and methods

3.1 Data acquisition

Seismic data used in this study were recorded from network 5H (COOL project), consisting of 40 broadband seismometers across the Oman Mountains, which were in operation for about 2 years and 5 months (from October 2013 to February 2016). Some of these seismometers were occasionally displaced, resulting in 45 station locations. Three different types of seismometers are exploited in this network, CMG-3ESP, Trillium120QA, STS-2, which were able to continuously record at 100 sps (Weidle et al., 2013). This network was deployed with the purpose of illuminating the 3D geometry and internal properties of the world's reference obducted oceanic crust, and the underlying continental lithosphere. The network is complemented by 13 permanent stations (network OM). These stations are equipped with an STS-2.5, Trillium 240, CMG-3TB, or Trillium 120 seismometer, operated by the local Earthquake Monitoring Center in Oman (Figure 1b).

3.2 Shear wave splitting (SWS)

In the past two decades, XKS phases have been extensively used to study seismic anisotropy (e.g., Kind et al., 1985; Silver and Chan, 1988; 1991; Savage and Silver, 1993). These phases have the advantage of being converted from P-to-S waves at the core-mantle boundary (CMB), meaning that splitting observed at the surface is the result of receiver-side anisotropy. In addition, with a near-vertical angle of incidence, these phases provide a relatively good lateral resolution beneath the monitoring stations. However, the signature of anisotropy in these phases is a vertically integrated effect from the CMB to the surface and thus they can provide limited constraints on the depth of anisotropy.

Seismograms used in this study were gathered from teleseismic events that occurred in epicentral distances of 85°-140° with a magnitude of Mw > 5.8, resulting in a total number of 10354 seismograms from 336 events. The National Earthquake Information Center (NEIC) provided the starting time and location of these teleseismic events. The IASP91 reference model was used to calculate the theoretical arrival times of XKS phases and to determine the time windows for the splitting analysis.

In this study, we use the SplitRacer code of Reiss and Rümpker (2017), an open-source MATLAB plugin, to perform the SWS analysis. Signals are filtered between 0.02 Hz and 0.2 Hz to improve the signal-to-noise ratio (SNR). The SNR threshold is set to be above 2.0. SplitRacer allows categorizing single splitting measurements, assigning a quality rating labeled as good, average, or poor to each measurement (Figure S1). This is done manually, taking into

consideration various factors such as the elliptical shape of the uncorrected particle motion, the percentage of the energy reduction on the transverse component, the size and shape of the 95% confidence contour, the distribution of φ and δt values from different chosen time windows (here 10 different time windows for each phase are selected), and the correlation between the fast and slow split shear waves components (see also Komeazi et al., 2023, section 2.2). If the uncorrected particle motion is apparently linear or the energy reduction of the T-component is negligible (less than 10%), the measurement is considered as "null". A null measurement could be attributed to either no anisotropy beneath the station or alignment of the initial polarization direction of the XKS phase with the fast/slow direction within the anisotropic medium.

In the first step, we search for splitting parameters (φ and δt) beneath each station that minimize the total energy of the T-component (Silver and Chan, 1991) for each individual XKS phase. These single SWS measurements are then used to confirm the azimuthal variation of the parameters. SplitRacer also allows for the joint splitting analysis of the XKS waveforms. Joint splitting analysis refers to simultaneously minimizing the total energy of the T-components of all XKS phases at one station. In case of a 90-degree periodicity of the splitting parameters versus back azimuth, which is indicative of a depth-dependent anisotropic media (Silver and Savage, 1994, Rümpker and Silver, 1998), we conduct a joint inversion, assuming a two-layer anisotropy. Due to its fast performance, a modified version of SplitRacer provided by Link et al. (2022) was used to conduct the two-layer joint splitting analysis. The correction of the T-component waveforms for splitting parameters is performed using an inverse splitting operator (Rümpker and Silver, 1998). The joint splitting parameters (for one- and two- layer models) for all stations are presented in Tables S1 and S2.

3.3 Ps-splitting analysis

In order to examine the presence of seismic anisotropy in the crust and its potential effect on the XKS splitting measurements (e.g., Latifi et al., 2018), we perform splitting analysis technique developed by Rümpker et al. (2014) on the Moho-converted P-to-S (Ps) phases observed in receiver function data computed at the same stations used for the XKS splitting analysis (Figure 1b). Teleseismic events in the epicentral distances 30°-95° are used for receiver function calculations. Preprocessing of receiver function analysis includes detrending and demeaning of waveforms, bandpass filtering from 0.02 to 2.0 Hz, and visual inspection of the waveforms to make sure about a clear P-wave arrivals. Receiver functions are then computed using time-domain deconvolution technique (Ligorria and Ammon, 1999).

The finite-frequency fast and slow shear waves overlap in weakly anisotropic media ($T >> \delta t$), resulting in a characteristic cosine-shaped move-out as a function of backazimuth in the Ps arrival time on radial receiver functions. In order to find the splitting parameters that result in a cosine-shape move-out, a grid search is applied in two steps (Rümpker et al., 2014). First, the best pair of the parameters (φ and δt) is obtained by stacking radial-component amplitudes along the sinusoidal move-out. Then, the estimated parameters are verified and improved by minimizing energy on transverse receiver functions.

4 *Results*

4.1 Individual XKS Splitting Measurements

After carefully choosing the input data based on teleseismic distance, magnitude, and SNR, a total number of 553 well-defined (quality good or average) individual XKS splitting measurements (1-29 measurements per station) were retained. Figure 2a depicts the individual SWS measurements at each station. The backazimuths of the events giving null measurements are shown in Figure S2. On the basis of the individual FPDs, the study region can be divided into three subregions: western, central, and eastern parts. The SGFZ and Hawasina Window (HW) are the geological features that separate the central area from the neighboring parts. However, this division does not imply that the observed anisotropy solely originates from the lithospheric domains. As will be discussed later, asthenosphere also contributes to it.

In the western part, the measurements performed at stations MOH, ASH, COO26, COO28, and COO29 are characterized by consistent φ and δt values. For the majority of the stations in this region, the orogenic belt and FPDs are aligned in the NNW-SSE/NW-SE direction, except for station BAN, located at the far north of western Oman, with some NE-SW–oriented FPDs. The delay times measured in the western part mainly range around 1.0 s. In the central region, the majority of high-quality measured FPDs fall within the range of N00°E to N045°E (NE-SW) and N125°E to N180°E (NW-SE). These observed variations in the FPDs could indicate the presence of multiple anisotropic layers. Additionally, most of the null measurements obtained in this study are from stations located in the central part, including COO12, 17, 20, 24, and 43.

Generally, more individual SWS measurements are obtained at the eastern part relative to the western part of the study area, not only due to more stations deployed, but also due to more measurements obtained per station. Most of the FPDs at the stations located in the eastern part are oriented in the WWN-EES, NW-SE and NNW-SSE directions. However, some stations also include FPDs with a NE-SW trend, which is parallel to the Absolute Plate Motion (APM) in the region as determined by Kreemer et al. (2014) in the No-Net-Rotation reference frame. The observed variation of the FPDs at stations such as BID, COO33 and COO53 indicate the

structural complexity underneath this region, which could be due to multiple sources of seismic anisotropy. A relatively sharp change in the direction of FPDs occurs at the SGFZ, from dominantly NW-SE orientation in the eastern side to dominantly NE-SW trend on the west. This pattern (also seen at the neighboring stations) might reflect short-wavelength variations in the upper mantle structure.

A further consideration is that some stations possess backazimuth-dependent splitting parameters. This might be due to the presence of multiple layers of anisotropy (Silver and Savage, 1994, Rümpker and Silver, 1998). Clear azimuthal variations can be seen at most of the stations in our study, particularly in the eastern and central parts (Figure S3). At several stations, the values of the fast polarization display systematic azimuthal variations with a period of ~90◦. Such patterns are consistent with a two-layer anisotropic model throughout the eastern and central part of the study area. As an example, Figure 2b shows the azimuthal variation in splitting parameters at station COO17. However, some stations located in the western parts (BAN, MDH, ASH) suffer from insufficient azimuthal coverage to infer the dependency of the splitting parameters on the backazimuth. Some stations exhibit large delay times (> 2 sec, up to 2.77 sec recorded at COO35) in the eastern part of the study area. These (apparent) large delay times could be the effect of depth-dependent anisotropy.

We also examine the case if the observed individual splitting measurements were generated from a single layer of anisotropy distributed at a certain depth. For this purpose, we follow the spatial coherency approach of Liu and Gao, (2011) modified by Gao and Liu, (2012). In this method, individual splitting measurements are projected to the ray piercing points, and then by calculating the spatial variation factors, the procedure determines the depth at which a maximum level of spatial coherency is reached. The anisotropy at this depth is taken as the main contributor to the observed shear wave splitting. We divided the study area into grids with grid point distance of 0.1° in both longitude and latitude directions. Then for each grid point the average φ and δt for all the splitting parameters within the Fresnel zone ($R_{fresnelzone} = 85 + 0.2 * depth$) is calculated. Finally, at each assumed depth the variation factor is computed. Our analysis suggests an optimal depth of 290 km (Figure S4a) for the source of anisotropy assuming a single layer of anisotropy. Compared to the real dataset in the study of Liu and Gao (2011), our results indicate that the variation factor exhibits a negligible dependence on depth. Furthermore, even by projecting the splitting parameters at the optimal depth (Figure S4b), there are still a considerable number of non-coherent splitting parameters. These results confirm that a one-layer model is not a precise approximation for the XKS observations at most of our stations.

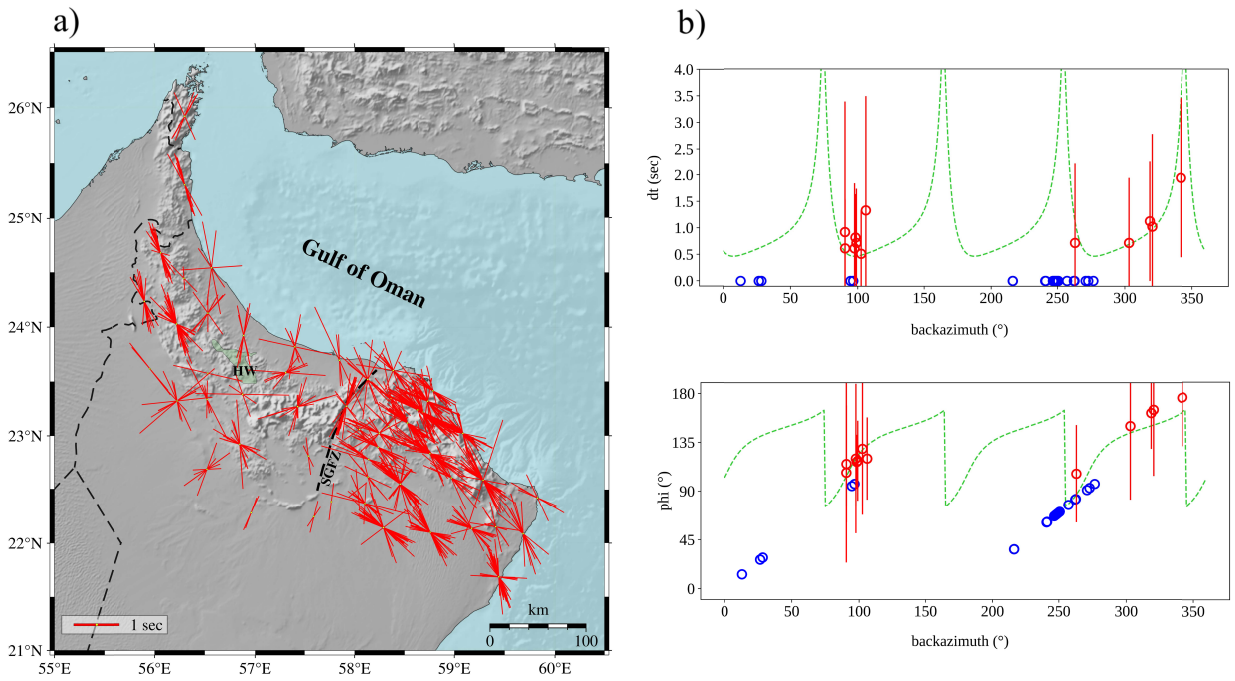

Figure 2. a) Individual splitting parameters of XKS waveforms are shown by red bars. They are oriented in the fast polarization direction with length proportional to the delay time. b) An example of backazimuthal variation at station COO17. The red and blue circles show non-null and null measurements. The green dash-lines are theoretical two-layer modeling parameters derived from joint inversion of XKS waveforms.

4.2 Joint inversion modeling

The joint-analysis approach described in Section 3.2 allows for the inversion of the XKS waveforms for one or two layers of anisotropy. Final joint splitting parameters from our XKS analysis are shown in Figure 3, along with more detailed parameters in Tables S1 and S2. As expected from the backazimuthal variations, we retrieve mostly two-layer models in the eastern and central parts (Table S2), whereas the western part is dominated by one-layer models (Table S1). At stations with two-layer models, T-component energy reduction is significantly improved relative to the one-layer model at the same stations (Figure S5). Insufficient coverage of back azimuths at a few stations (SOH, COO25, COO28, COO27 and COO23) makes it difficult to draw definitive conclusions about having depth-dependent anisotropy beneath these stations. The joint XKS splitting delay times are on average around 1.1 s for one-layer models, 0.83 for upper layers and 0.76 for lower layers. The slightly larger delay times in the upper layer compared to the lower layer suggest that the study area is more influenced by upper mantle and lithospheric anisotropy. Furthermore, at central parts, the delay times are much smaller than the other parts of the study area. In the eastern part, the fast symmetry axes of the upper layer dominantly trend

WWN-EES, consistent with the trend of the fast axes of the one-layer model beneath the stations in the western part. The lower layer fast axes appear to be well-clustered toward the NNE-SSW/N-S direction. The difference between the upper-layer fast orientations and one-layer models is small, indicating that the improvement in data fit is mainly due to the contribution of the lower layer. A lateral variation in the upper layer FPDs occurs along the strike of the mountain range changing from a WWN-EES trend in the eastern part to a NE-SW trend in central part at the SGFZ that then changes to a dominantly NW-SE direction in the west.

Rümpker et al. (2023) argued that the results of layered anisotropy could be highly non-unique and emphasized the need for prior information from the region to validate these findings. In our study, we conducted several tests by incorporating prior information from the study area to fix the upper layer (in the direction of mafic intrusions) or lower layer (in the direction of APM) FPDs. Our tests confirm the two-layer parameters presented in this study (Figure S6 and S7).

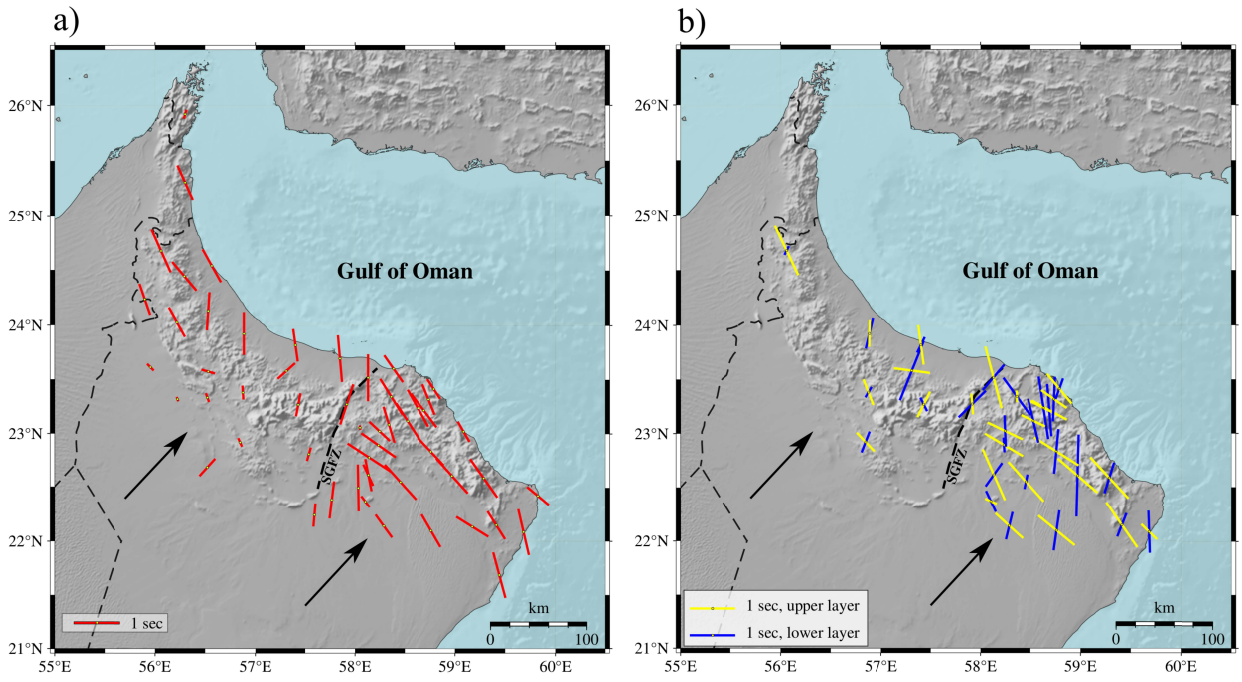

Figure 3. a) one-layer splitting parameters obtained from joint-splitting analysis of XKS waveforms, shown with red bars, b) two-layer splitting parameters obtained from joint-splitting analysis of XKS waveforms, shown with yellow (upper layer) and blue (lower layer) bars. On both maps, the bars are oriented in the fast polarization direction with length proportional to the delay time. Black arrows illustrate the direction of the APM.

4.3 Effects of crustal anisotropy

Out of all the stations where we applied the Ps-splitting method, only 14 stations fulfilled the requirement of sufficient azimuthal coverage, which is necessary to obtain reliable results in Ps-splitting method. In Figure 5, the purple bars represent these computed splitting parameters. At stations situated on the western side of the SGFZ, the orogen-parallel splitting parameters are consistent with the upper crust anisotropy from surface waves (Wiesenberg et al., 2022). On the eastern side of the SGFZ, however, FPDs are rather NE-SW and thus more consistent with lower crustal anisotropy observed from surface waves. This suggests a dominant upper and lower crustal anisotropy in the central and eastern parts of the study area, respectively.

Using crustal anisotropy results from the Ps-splitting (an example is illustrated in Figure S8), we examine the effect of the crustal anisotropy on the XKS splitting observations at several stations with adequate azimuthal coverage. At these locations, we search for two-layer models by following 2 schemes. I) two-layer modeling by fixing the fast direction of the upper layer in the direction of the crustal anisotropy. II) two-layer modeling after removing the crustal anisotropy effect from the waveforms.

In scheme I, the joint inversion of the XKS waveforms is conducted for a two-layer model in which the parameters of the upper layer are constrained to vary around the parameters obtained from the Ps-splitting. Then the joint inversion gives the delay time of the upper layer and the delay time and fast axis of the lower layer. In scheme II, in the first step, the XKS waveforms are corrected according to the splitting parameters obtained by the Ps-splitting analysis of receiver functions. The required mathematical equations to correct the waveforms for a certain φ and δt are explained in detail in Rümpker et al. (2023). After correcting the waveforms for the crustal anisotropy parameters, we applied the joint splitting method for a two-layer anisotropy.

The results of this inversion for both schemes are shown in Figure 4 along with the two-layer joint splitting parameters obtained without constraining the crustal anisotropy for the same stations. Only 6 stations delivered reliable layered models by constraints from crustal anisotropy. Due to a more effective reduction in average T-component energy provided by scheme II, the splitting parameters derived from this scheme are selected as the final two-layer parameters. As illustrated in Figure 4, for stations COO16 and COO20, situated in the western part of the SGFZ, the fast axes given by scheme II are nearly identical to those derived from the inversions without crustal constraint. Nonetheless, the delay times at both stations increased under scheme II. In contrast, for stations COO32 and COO37, the delay times of the upper layer decreased in scheme II compared to the inversions without crustal constraint. Additionally, at stations COO05 and COO51, distinct anisotropic layers are observed in various schemes.

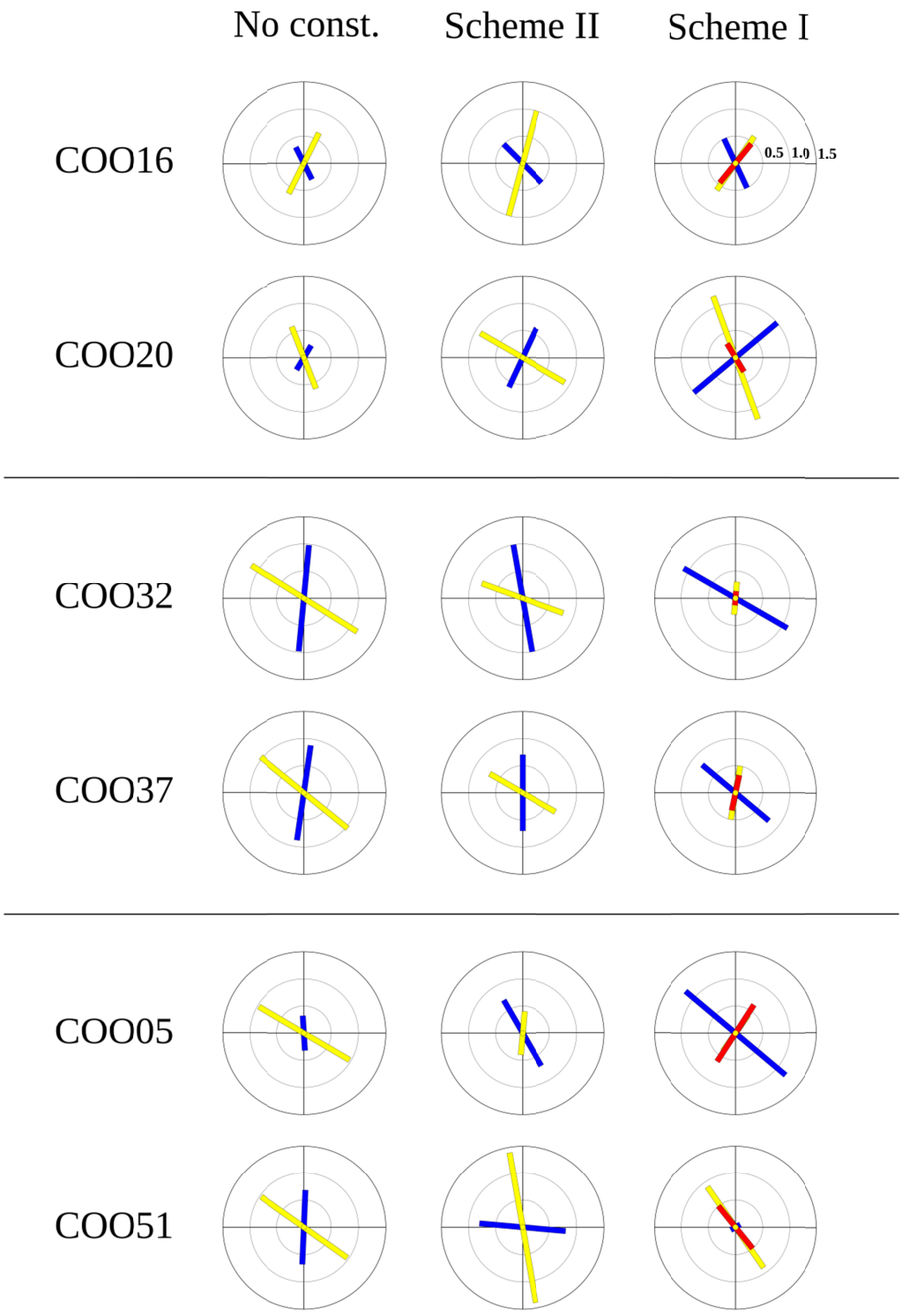

Figure 4. Scheme I) the fast polarization directions of the upper layer are constrained to vary around the parameters obtained from the Ps-splitting. Scheme II) XKS waveforms are first corrected by Ps-splitting results, and then two-layer joint splitting analysis is performed on corrected XKS waveforms. Ps-splitting parameters indicated by red bars. The upper- and lower-

layer joint splitting parameters are shown with yellow and blue bars. The bars are oriented in the obtained fast directions, and their length is proportional to the delay time.

5 Discussion

A shear wave splitting analysis along northern Oman is provided in this study by using a dense network of stations. We discuss the possible causes of seismic anisotropy beneath northern Oman in the context of the tectonic setting of the region. We examine the effects of extensive processes of orogeny, rifting and basin formation at a continental margin on the lithosphere beneath the northern Oman. The presented results of the XKS splitting analysis show a depth-dependent anisotropic pattern in the splitting parameters at the majority of the stations.

Many of the delay times are too large to be attributed exclusively to the lithosphere. Considering the maximum delay times measured in this study, which are of the order of ~2.5 s, a maximum thickness of ~125–250 km can be expected for the anisotropic layer, assuming an average anisotropy strength of 2–4% (e.g., Savage, 1999; Helffrich, 1995) and an average Vs of ~4 km/s for the upper mantle (Weidle et al., 2022). Weidle et al. (2023) suggest that the lithosphere thickness beneath our study region is in the order of ~80–120 km. A uniform anisotropic layer with a mean value of 4% of anisotropy can explain the average delay time value of ~1.0 sec observed in the region. However, as explained in previous section, a single layer of anisotropy cannot explain the lateral and azimuthal variations in the observed XKS splitting measurements. Therefore, we need to discuss the observations by considering both the lithospheric and sub-lithospheric sources of anisotropy.

In Figure 5, we summarize the inferred depth-dependent anisotropic model that is obtained for the entire region by joint inversion of the XKS data and considering the effect of the crustal anisotropy as constrained by the Ps-splitting analysis.

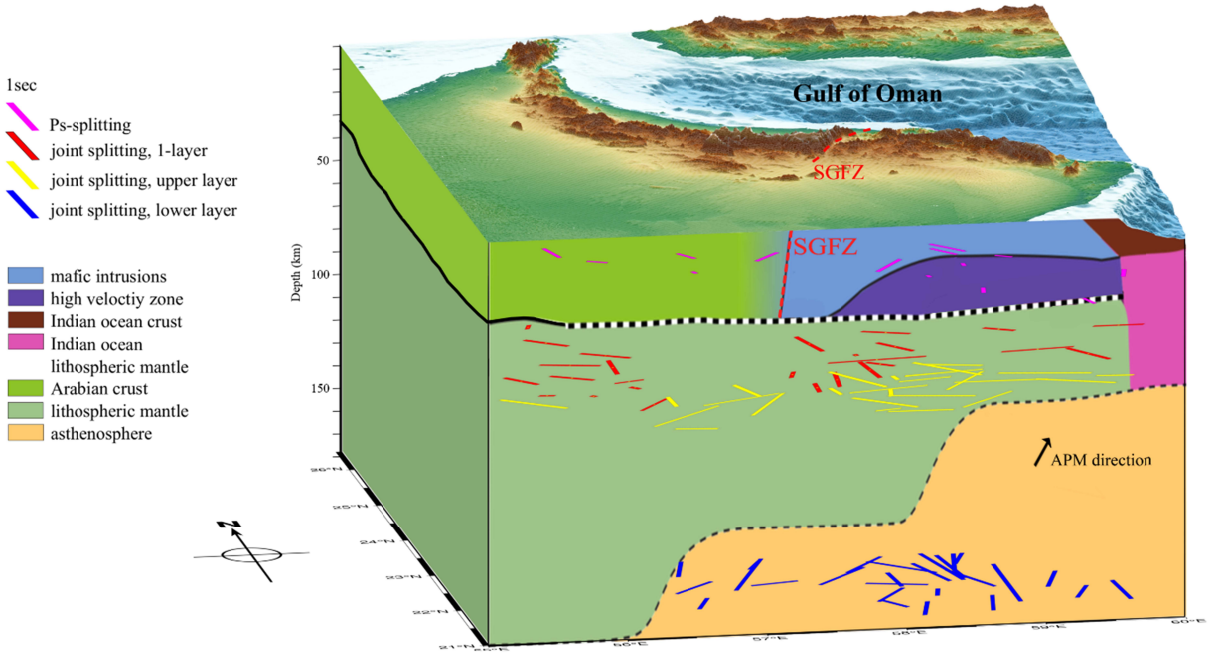

Figure 5. Schematic visualization summarizing the anisotropy parameters observed beneath the study area using the Ps-splitting and Joint splitting methods. Bars in different colors as described in the legend show the orientation of the fast polarization directions and their length are proportional to the delay times. The schematic geophysical features depicted in the depth cross-section are derived from Weidle et al. (2023).

5.1 Lithospheric deformation

The one-layer joint splitting parameters determined in our study (Figure 3a) can be categorized into NW-SE and NNE-SSW/NE-SW trending FPDs. A strong mountain range parallel pattern of the one-layer FPDs is observed in the study area, which is likely due to the compressional forces as a result of Neo-Tethys closure, suggesting the presence of the "fossil" anisotropic fabric in the lithospheric mantle beneath northern Oman. However, a clear distinction regarding the splitting parameters occurs at Semail Gap Fault Zone (SGFZ). On the eastern side of the SGFZ, FPDs are trending NW-SE, whereas the FPDs are mostly oriented NE-SW west of the SGFZ. Finally, Moving from HW towards western part of the study area, the FPDs revert back to the NW-SE trend. This patterns of the FPDs, portraits the central part as a different part relative to the neighboring areas. The variation in our observations in the central part possibly stem from complexity as a result of locating within the transition zone (see also section 2). The entire study area underwent extensive lithospheric modification during the Permian breakup of Pangea – first by extension and breakup to the SE (Indian Ocean) and NW (Neo-Tethys) and second by mafic modification, on eastern domain of SGFZ, which is characterized by a strongly volcanic margin.

In the western parts of the study area, the one-layer FPDs (with NW-SE orientation) are very similar, suggesting the overall uniformity of the anisotropic structure at depth. In comparison to the previous study (Pilia et al., 2021), their averaged values agree well with our joint splitting parameters for one-layer models in the same region or stations (Figure S9). At different stations, mean split times range from 0.6 to 1.6 s, with smallest values suggesting weak anisotropy, a relatively thin anisotropic layer where the crust may have played a significant role, or possibly two perpendicular anisotropic layers that cancel out each other's effects.

The observed 90° periodicity in the backazimuthal variation of the splitting parameters at some stations, particularly in the central and eastern parts (Figure 2b and Figure S3), prompted us to examine two-layer models with horizontal symmetry axes. The two-layer joint splitting parameters are shown in Figure 3b. A NW-SE trend is observed for the upper layer and NE-SW/NNE-SSW for the lower layer, which we attribute to the lithospheric mantle and asthenosphere, respectively (Figure 5). As delay times of the lower layer increase from west to east, we infer a thickening of the anisotropic layer (asthenosphere) under a thinning lithosphere.

The majority of the FPDs of the upper layers, mostly in the eastern side of the SGFZ, as well as the FPDs of the one-layer models in the entire region are subparallel to the main tectonic trends visible at the surface, resulting from compressional tectonics during Arabia-Eurasia convergence. In addition, on the eastern side of the SGFZ, emplacement of the mafic intrusions in the ~WNW-ESE direction (Weidle et al., 2023) can partially explain the observed NW-SE apparent anisotropy in this area. Furthermore, The SGFZ is discussed in previous studies as a distinguishing tectonic feature. For instance, the abundance of mafic rocks in the Saih Hatat Dome (SHD) has been attributed to the plate breakup (Chauvet et al., 2009) and since the Jabal Akhdar Dome (JAD) region was minimally impacted by the mafic rocks, the SGFZ is thought to be acting as a structural barrier at the time, as proposed by Scharf et al. (2019). In the absence of mafic intrusions on the western side of the SGFZ, the upper- and lower- layer delay times are comparable, suggesting a thicker lithospheric mantle beneath the central parts. Therefore, given the NE-SW trend of the one-layer FPDs in the central part, we argue the crustal anisotropy resulting from the NE-SW extension (Figure 5) plays a significant role in this area. However, in the west, no significant backazimuthal variation is observed and the predominant NW-SE trend of the one-layer FPDs arise from the thick and old lithospheric mantle, which undergone the compressional tectonic regime.

The average delay times for the crustal anisotropy as obtained using the Ps-splitting analysis are in good agreement with observations reported from other regions, which is of order of ~0.3–0.5 sec (Barruol and Mainprice, 1993; Silver, 1996). The orogen parallel pattern of the Ps-splitting results for the crustal anisotropy resemble those for the upper-layer joint splitting results as well as the azimuthal anisotropy estimated by surface wave tomography (Wiesenberg et al., 2022; Weidle et al., 2023). The analysis of crustal anisotropy has revealed more insights into the deep

structure of the eastern and central regions. At stations COO32 and COO37 in the eastern region, it appears that the crust and lithospheric mantle have undergone coherent deformations, resulting in smaller delay times for the upper layer when correcting the XKS waveforms for crustal anisotropy. In contrast, stations COO51 and COO05 yield completely different models relative to the case with no crustal constraints, indicating the complexity beneath this area. West of the SGFZ, stations COO16 and COO20 show a nearly orthogonal fast axis between the crustal anisotropic layer and the lower layer, thereby weakening the effect of the bottom layers. This could explain the relatively small joint splitting delay times for the stations located west of the SGFZ (e.g., COO24 and 13), despite the fact that the individual measurements contain much larger delay times. These findings provide insights into the complex dynamics of the crust and mantle across the study area.

5.2 Large-scale Mantle Flow due to the plate motion and subduction

A basic assumption regarding the shear (basal drag) in the transition layer between the lithosphere and the underlying asthenosphere is that it is influenced by the APM, causing the orientation of the olivine a-axis to be subparallel to the APM direction (Silver, 1996; Zhang and Karato, 1995). The development of the basal drag fabric is believed to be influenced by plate velocity (Debayle and Ricard, 2013), wherein slow-moving plates are unable to generate a sufficiently strong basal drag fabric to produce significant anisotropy. While the plate convergence speed reached 6 cm/yr during the Cretaceous (Agard et al., 2007), GPS measurements by Vernant et al. (2004) and Khorrami et al. (2019) showed a rate of approximately 27 mm/yr for the current Arabian plate motion. However, there is no evidence to suggest that this reduction in velocity would impact the pervasive anisotropy fabric developed by the basal drag in the direction of APM.

The predominant observed fast polarization directions (FPDs) within the lower anisotropic layer (N7°–55°E) in our study exhibit an approximate alignment with the absolute plate motion (APM) direction (~N47°E) in northern Oman, assuming the no-net-rotation reference frame for plate motion (Kreemer et al., 2014). The slight discrepancy between the observed FPDs in the lower layer and the APM can be attributed to the northerly movement of the lithospheric mantle. This north component of the lithospheric mantle could be due to the northward dipping subduction zone within the Neo-Tethys Ocean (Tavani et al., 2020), which resulted in a northward deviation of the FPDs caused by the APM. The same argument applies to the FPDs observed at stations COO08, COO09, and COO10 in the southeastern region, which are predominantly oriented in NNE-SSW direction. The measured splitting parameters at these stations arise from a combination of mantle flow and minor influences of lithospheric anisotropy.

6 Conclusions

Using a combination of data from both permanent and temporary seismic networks, we studied seismic anisotropy beneath northern Oman. The majority of the stations located in the eastern and central parts of the study area exhibit systematic azimuthal variations of the fast polarization directions (FPDs) of splitting analysis with a 90° periodicity. These azimuthal variations suggest the presence of at least two layers of anisotropy beneath this region. On the other hand, for the stations located to NW, our observations suggest dominantly one-layer anisotropic models. Overall, most of the upper layer in the two-layer models in the east, coincident with the fast directions of the one-layer models to west, which in turn are sub-parallel to the major tectonic trends and boundaries visible at the surface. This, along with the significant variation in the FPDs between some neighboring stations suggests that the lithospheric structural alignments are the main source of anisotropy of the upper layer. The observed orogen-parallel anisotropy supports the idea of frozen-in lithospheric mantle anisotropy resulting from the compressional forces in northern Oman. In the east, the combination of thin lithosphere and mafic intrusions effects are dominant, making the NW-SE trend. Within the central part, the presence of a thicker lithosphere empowers the role of crustal anisotropy. A relatively weak apparent anisotropy in the central part might be due to complex lateral and depth variation of the anisotropic structure in the lithosphere. In the west, the NW-SE FPDs highlight the significant role of the thick and old lithosphere of the Arabian plate in the resulting anisotropy. The predominantly NE-SW trend of the lower layer anisotropy in the central and southeastern part of the study area is parallel to the absolute plate motion (APM). Therefore, we argue that this anisotropic fabric is created by the large-scale mantle flow beneath northern Oman due to the plate motion.

Acknowledgments

We would like to thank the GEOFON data repository of Deutsches Geoforschungszentrum Potsdam (GFZ) for providing data from the temporary seismic network 5H. Instrumentation for the COOL experiment was provided by the German Geophysical Instrument Pool Potsdam (GIPP). AK expresses gratitude for the support received from a Goethe-University scholarship provided through the department of Geosciences/Geography.

Open Research

Data: Data from the networks 5H are accessible from GEOFON/GFZ via the following link: http://doi.org/10.7914/SN/5H_2013. The information about the origin time and location of the teleseismic events were taken from the National Earthquake Information Center (NEIC) these are available on the U.S. Geological Survey (USGS) website at http://earthquake.usgs.gov.

Software: The data analysis was performed using the MATLAB code SplitRacer. The code is available via the link: https://www.geophysik.uni-frankfurt.de/64002762/software.

Graphs: The figures presented in the paper were generated using the PyGMT (https://www.pygmt.org).

References

Agard P, Jolivet L, Vrielynck B, Burov E, Monie P. Plate acceleration: The obduction trigger?. Earth and Planetary Science Letters. 2007 Jun 30;258(3-4):428-41. https://doi.org/10.1016/j.epsl.2007.04.002

Al-Lazki AI, Al-Damegh KS, El-Hadidy SY, Ghods A, Tatar M. Pn-velocity structure beneath Arabia–Eurasia Zagros collision and Makran subduction zones. Geological Society, London, Special Publications. 2014 Apr 4;392(1):45-60. https://doi.org/10.1144/SP392.3

Allen PA. The Huqf Supergroup of Oman: basin development and context for Neoproterozoic glaciation. Earth-Science Reviews. 2007 Oct 1;84(3-4):139-85. https://doi.org/10.1016/j.earscirev.2007.06.005

Ambrose TK, Searle MP. 3D structure of the northern Oman UAE ophiolite: Widespread, shortlived, suprasubduction zone magmatism. Tectonics. 2019 Jan;38(1):233-52. https://doi.org/10.1029/2018TC005038

Barruol G, Souriau A, Vauchez A, Diaz J, Gallart J, Tubia J, Cuevas J. Lithospheric anisotropy beneath the Pyrenees from shear wave splitting. Journal of Geophysical Research: Solid Earth. 1998 Dec 10;103(B12):30039-53. https://doi.org/10.1029/98JB02790

Barruol G, Mainprice D. A quantitative evaluation of the contribution of crustal rocks to the shear-wave splitting of teleseismic SKS waves. Physics of the Earth and Planetary Interiors. 1993 Jul 1;78(3-4):281-300. https://doi.org/10.1016/0031-9201(93)90161-2

Celli NL, Lebedev S, Schaeffer AJ, Gaina C. African cratonic lithosphere carved by mantle plumes. Nature communications. 2020 (a) Jan 3;11(1):92. https://doi.org/10.1038/s41467-019-13871-2

Celli NL, Lebedev S, Schaeffer AJ, Ravenna M, Gaina C. The upper mantle beneath the South Atlantic Ocean, South America and Africa from waveform tomography with massive data sets. Geophysical Journal International. 2020 (b) Apr;221(1):178-204. https://doi.org/10.1093/gji/ggz574

Chauvet F, Dumont T, Basile C. Structures and timing of Permian rifting in the central Oman Mountains (Saih Hatat). Tectonophysics. 2009 Oct 1;475(3-4):563-74. https://doi.org/10.1016/j.tecto.2009.07.008

Cozzi A, Rea G, Craig J. From global geology to hydrocarbon exploration: Ediacaran-Early Cambrian petroleum plays of India, Pakistan and Oman. Geological Society, London, Special Publications. 2012;366(1):131-62. https://doi.org/10.1144/SP366.14

Debayle E, Ricard Y. Seismic observations of large-scale deformation at the bottom of fast-moving plates. Earth and Planetary Science Letters. 2013 Aug 15;376:165-77. https://doi.org/10.1016/j.epsl.2013.06.02

Gao SS, Liu KH. AnisDep: A FORTRAN program for the estimation of the depth of anisotropy using spatial coherency of shear-wave splitting parameters. Computers & Geosciences. 2012 Dec 1;49:330-3. https://doi.org/10.1016/j.cageo.2012.01.020

Glennie KW. Geology of the Oman mountains. Verhandelingen van het Koninklink Nederlands Geologisch Mijnbouwkundig Genootchachp. 1974;1:423.

Guilmette C, Smit MA, van Hinsbergen DJ, Gürer D, Corfu F, Charette B, Maffione M, Rabeau O, Savard D. Forced subduction initiation recorded in the sole and crust of the Semail Ophiolite of Oman. Nature Geoscience. 2018 Sep;11(9):688-95. https://doi.org/10.1038/s41561-018-0209-2

Hacker BR, Mosenfelder JL, Gnos E. Rapid emplacement of the Oman ophiolite: Thermal and geochronologic constraints. Tectonics. 1996 (a) Dec;15(6):1230-47. https://doi.org/10.1029/96TC01973

Hacker BR, Mosenfelder JL. Metamorphism and deformation along the emplacement thrust of the Samail ophiolite, Oman. Earth and Planetary Science Letters. 1996 (b) Nov 1;144(3-4):435-51. https://doi.org/10.1016/S0012-821X(96)00186-0

Helffrich G. Lithospheric deformation inferred from teleseismic shear wave splitting observations in the United Kingdom. Journal of Geophysical Research: Solid Earth. 1995 Sep 10;100(B9):18195-204. https://doi.org/10.1029/95JB01572

Hess HH. Seismic anisotropy of the uppermost mantle under oceans. Nature. 1964 Aug 8;203(4945):629-31. https://doi.org/10.1038/203629a0

Holtzman BK, Kendall JM. Organized melt, seismic anisotropy, and plate boundary lubrication. Geochemistry, Geophysics, Geosystems. 2010 Dec;11(12). https://doi.org/10.1029/2010GC003296

Khorrami F, Vernant P, Masson F, Nilfouroushan F, Mousavi Z, Nankali H, Saadat SA, Walpersdorf A, Hosseini S, Tavakoli P, Aghamohammadi A. An up-to-date crustal deformation map of Iran using integrated campaign-mode and permanent GPS velocities. Geophysical Journal International. 2019 May;217(2):832-43. https://doi.org/10.1093/gji/ggz045

Kind R, Kosarev GL, Makeyeva LI, Vinnik LP. Observations of laterally inhomogeneous anisotropy in the continental lithosphere. Nature. 1985 Nov 28;318(6044):358-61. https://doi.org/10.1038/318358a0

Komeazi A, Kaviani A, Rümpker G. Mantle anisotropy in NW Namibia from XKS splitting: Effects of asthenospheric flow, lithospheric structures, and magmatic underplating. Geophysical Research Letters. 2023 Feb:e2022GL102119. https://doi.org/10.1029/2022GL102119

Koulakov I, Burov E, Cloetingh S, El Khrepy S, Al-Arifi N, Bushenkova N. Evidence for anomalous mantle upwelling beneath the Arabian Platform from travel time tomography inversion. Tectonophysics. 2016 Jan 23;667:176-88. https://doi.org/10.1016/j.tecto.2015.11.022

Kreemer C, Blewitt G, Klein EC. A geodetic plate motion and Global Strain Rate Model. Geochemistry, Geophysics, Geosystems. 2014 Oct;15(10):3849-89. https://doi.org/10.1002/2014GC005407

Latifi, K., Kaviani, A., Rümpker, G., Mahmoodabadi, M., Ghassemi, M.R. and Sadidkhouy, A., 2018. The effect of crustal anisotropy on SKS splitting analysis—synthetic models and real-data observations. *Geophysical Journal International*, *213*(2), pp.1426-1447. https://doi.org/10.1093/gji/ggy053

Ligorría JP, Ammon CJ. Iterative deconvolution and receiver-function estimation. Bulletin of the seismological Society of America. 1999 Oct 1;89(5):1395-400. https://doi.org/10.1785/BSSA0890051395.

Link F, Reiss MC, Rümpker G. An automatized XKS-splitting procedure for large data sets: Extension package for SplitRacer and application to the USArray. Computers & Geosciences. 2022 Jan 1;158:104961. https://doi.org/10.1016/j.cageo.2021.104961

Liu KH, Gao SS. Estimation of the depth of anisotropy using spatial coherency of shear-wave splitting parameters. Bulletin of the Seismological Society of America. 2011 Oct 1;101(5):2153-61. https://doi.org/10.1785/0120100258

Long MD, Silver PG. Shear wave splitting and mantle anisotropy: Measurements, interpretations, and new directions. Surveys in Geophysics. 2009 Oct;30:407-61. https://doi.org/10.1007/s10712-009-9075-1

McKenzie, D., 1979. Finite deformation during fluid flow. *Geophysical Journal International*, *58*(3), pp.689-715. https://doi.org/10.1111/j.1365-246X.1979.tb04803.x

Nicolas A, Boudier F, Ildefonse B, Ball E. Accretion of Oman and United Arab Emirates ophiolite–Discussion of a new structural map. Marine Geophysical Researches. 2000 May;21:147-80. https://doi.org/10.1023/A:1026769727917

Nicolas A, Boudier F, Ildefonse B. Evidence from the Oman ophiolite for active mantle upwelling beneath a fast-spreading ridge. Nature. 1994 Jul 7;370(6484):51-3. https://doi.org/10.1038/370051a0

Ninkabou D, Agard P, Nielsen C, Smit J, Gorini C, Rodriguez M, Haq B, Chamot-Rooke N, Weidle C, Ducassou C. Structure of the offshore obducted Oman margin: emplacement of Semail ophiolite and role of tectonic inheritance. Journal of Geophysical Research: Solid Earth. 2021 Feb;126(2):2020JB020187. https://doi.org/10.1029/2020JB020187

Pilia S, Hu H, Ali MY, Rawlinson N, Ruan A. Upper mantle structure of the northeastern Arabian Platform from teleseismic body-wave tomography. Physics of the Earth and Planetary Interiors. 2020 (a) Oct 1;307:106549. https://doi.org/10.1016/j.pepi.2020.106549

Pilia S, Jackson JA, Hawkins R, Kaviani A, Ali MY. The southern Zagros collisional orogen: new insights from transdimensional trees inversion of seismic noise. Geophysical Research Letters. 2020 (b) Feb 28;47(4):e2019GL086258. https://doi.org/10.1029/2019GL086258

Pilia S, Kaviani A, Searle MP, Arroucau P, Ali MY, Watts AB. Crustal and mantle deformation inherited from obduction of the Semail ophiolite (Oman) and continental collision (Zagros). Tectonics. 2021 Jun;40(6):e2020TC006644. https://doi.org/10.1029/2020TC006644

Pillevuit A, Marcoux J, Stampfli G, Baud A. The Oman Exotics: a key to the understanding of the Neotethyan geodynamic evolution. Geodinamica Acta. 1997 Nov 1;10(5):209-38. https://doi.org/10.1080/09853111.1997.11105303

Priestley K, McKenzie D, Barron J, Tatar M, Debayle E. The Zagros core: Deformation of the continental lithospheric mantle. Geochemistry, Geophysics, Geosystems. 2012 Nov;13(11). https://doi.org/10.1029/2012GC004435

Reiss MC, Rümpker G. SplitRacer: MATLAB code and GUI for semiautomated analysis and interpretation of teleseismic shear-wave splitting. Seismological Research Letters. 2017 Mar 1;88(2A):392-409. https://doi.org/10.1785/0220160191

Rioux M, Garber J, Bauer A, Bowring S, Searle M, Kelemen P, Hacker B. Synchronous formation of the metamorphic sole and igneous crust of the Semail ophiolite: New constraints on the tectonic evolution during ophiolite formation from high-precision U–Pb zircon geochronology. Earth and Planetary Science Letters. 2016 Oct 1;451:185-95. https://doi.org/10.1016/j.epsl.2016.06.051

Ruban DA, Al-Husseini MI, Iwasaki Y. Review of Middle east Paleozoic plate tectonics. GeoArabia. 2007 Jul 1;12(3):35-56. https://doi.org/10.2113/geoarabia120335

Rümpker G, Kaviani A, Latifi K. Ps-splitting analysis for multilayered anisotropic media by azimuthal stacking and layer stripping. Geophysical Journal International. 2014 Oct 1;199(1):146-63. https://doi.org/10.1093/gji/ggu154

Rümpker, G., Kaviani, A., Link, F., Reiss, M. C., & Komeazi, A. Testing Observables for Teleseismic Shear-Wave Splitting Inversions: Ambiguities of Intensities, Parameters, and Waveforms. Ann. Geophys. 2023 May. https://doi.org/10.4401/ag-8870

Rümpker G, Silver PG. Apparent shear-wave splitting parameters in the presence of vertically varying anisotropy. Geophysical Journal International. 1998 Dec 1;135(3):790-800. https://doi.org/10.1046/j.1365-246X.1998.00660.x

Savage MK. Seismic anisotropy and mantle deformation: what have we learned from shear wave splitting?. Reviews of Geophysics. 1999 Feb;37(1):65-106. https://doi.org/10.1029/98RG02075

Savage MK, Silver PG. Mantle deformation and tectonics: constraints from seismic anisotropy in the western United States. Physics of the Earth and Planetary Interiors. 1993 Jul 1;78(3-4):207-27. https://doi.org/10.1016/0031-9201(93)90156-4

Scharf A, Mattern F, Moraetis D, Callegari I, Weidle C. Postobductional kinematic evolution and geomorphology of a major regional structure—The Semail Gap Fault Zone (Oman Mountains). Tectonics. 2019 Aug;38(8):2756-78. https://doi.org/10.1029/2019TC005588

Searle MP, Malpas J. Structure and metamorphism of rocks beneath the Semail ophiolite of Oman and their significance in ophiolite obduction. Earth and Environmental Science Transactions of the Royal Society of Edinburgh. 1980;71(4):247-62. https://doi.org/10.1017/S0263593300013614

Searle M, Cox J. Tectonic setting, origin, and obduction of the Oman ophiolite. Geological Society of America Bulletin. 1999 Jan 1;111(1):104-22. https://doi.org/10.1130/0016-7606(1999)111%3C0104:TSOAOO%3E2.3.CO;2

Shad Manaman N, Shomali H, Koyi H. New constraints on upper-mantle S-velocity structure and crustal thickness of the Iranian plateau using partitioned waveform inversion. Geophysical Journal International. 2011 Jan 1;184(1):247-67. http://dx.doi.org/10.1111/j.1365-246X.2010.04822.x

Silver PG, Savage MK. The interpretation of shear-wave splitting parameters in the presence of two anisotropic layers. Geophysical Journal International. 1994 Dec 1;119(3):949-63. https://doi.org/10.1111/j.1365-246X.1994.tb04027.x

Silver PG. Seismic anisotropy beneath the continents: Probing the depths of geology. Annual review of earth and planetary sciences. 1996 May;24(1):385-432. https://doi.org/10.1146/annurev.earth.24.1.385

Silver PG, Chan WW. Implications for continental structure and evolution from seismic anisotropy. Nature. 1988 Sep 1;335(6185):34-9. https://doi.org/10.1038/335034a0

Silver PG, Chan WW. Shear wave splitting and subcontinental mantle deformation. Journal of Geophysical Research: Solid Earth. 1991 Sep 10;96(B10):16429-54. https://doi.org/10.1029/91JB00899

Tavani S, Corradetti A, Sabbatino M, Seers T, Mazzoli S. Geological record of the transition from induced to self-sustained subduction in the Oman Mountains. Journal of Geodynamics. 2020 Jan 1;133:101674. https://doi.org/10.1016/j.jog.2019.101674

Tippit PR, Pessagno Jr EA, Smewing JD. The biostratigraphy of sediments in the volcanic unit of the Samail ophiolite. Journal of Geophysical Research: Solid Earth. 1981 Apr 10;86(B4):2756-62. https://doi.org/10.1029/JB086iB04p02756

Vernant P, Nilforoushan F, Hatzfeld D, Abbassi MR, Vigny C, Masson F, Nankali H, Martinod J, Ashtiani A, Bayer R, Tavakoli F. Present-day crustal deformation and plate kinematics in the Middle East constrained by GPS measurements in Iran and northern Oman. Geophysical Journal International. 2004 Apr 1;157(1):381-98. https://doi.org/10.1111/j.1365-246X.2004.02222.x

Weidle C, Agard P, Meier T, Ducassou C, El-Hussain I. Cool (crust of the oman ophiolite and its lithosphere) seismic network. GEOFON Data Archive. 2013. https://doi.org/10.7914/SN/5H_2013

Weidle C, Wiesenberg L, El-Sharkawy A, Krüger F, Scharf A, Agard P, Meier T. A 3-D crustal shear wave velocity model and Moho map below the Semail Ophiolite, eastern Arabia. Geophysical Journal International. 2022 Nov;231(2):817-34. https://doi.org/10.1093/gji/ggac223

Weidle, C.; Wiesenberg, L.; Scharf, A.; Agard, P.; El-Sharkawy, A.; Krüger, F. & Meier, T. Lithospheric evolution of eastern Arabia based on surface wave and receiver function analyses. Earth and Planetary Science Letters, Elsevier BV, 2023, 611, 118145. https://doi.org/10.1016/j.epsl.2023.118145

Wiesenberg, L.; Weidle, C.; El-Sharkawy, A.; Timko, M.; Lebedev, S. & Meier, T. Measuring the phase of ambient noise cross correlations: anisotropic Rayleigh and Love wave tomography across the Oman Mountains. Geophysical Journal International, 2022, *231*, 1233-1251. https://doi.org/10.1093/gji/ggac232

Zhang S, Karato SI. Lattice preferred orientation of olivine aggregates deformed in simple shear. Nature. 1995 Jun 29;375(6534):774-7. https://doi.org/10.1038/375774a0

Figure1.

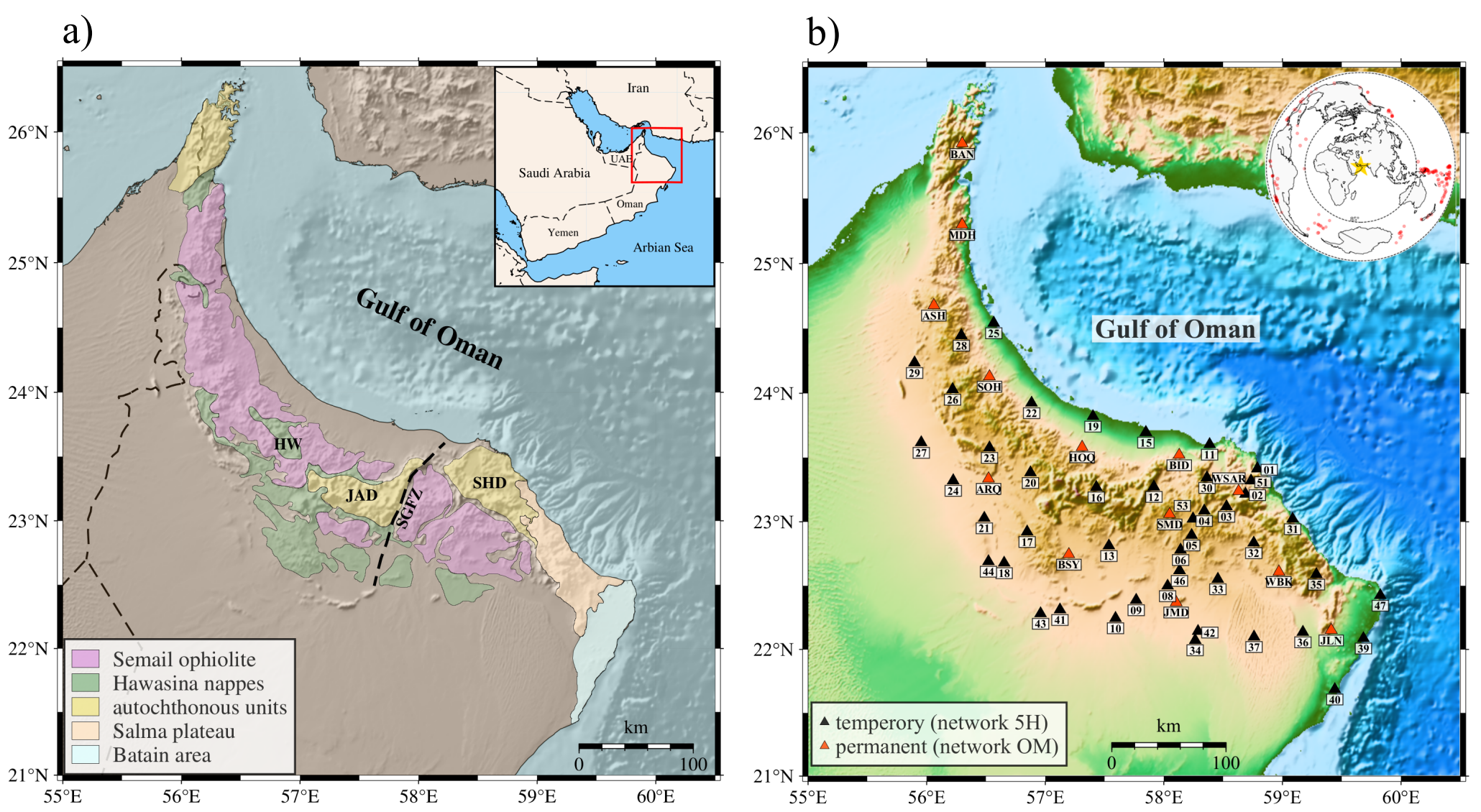
a)
b)
Gulf of Oman
Iran
Saudi Arabia
UAE
Oman
Yemen
Arbian Sea
HW
JAD
SGFZ
SHD
Semail ophiolite
Hawasina nappes
autochthonous units
Salma plateau
Batain area
km
0
100
temperory (network 5H)
permanent (network OM)
BAN
MDH
ASH
SOH
ARQ
HOQ
BID
WSAR
SMD
BSY
WBK
JMD
JLN
26°N
25°N
24°N
23°N
22°N
21°N
55°E
56°E
57°E
58°E
59°E
60°E

Figure2.

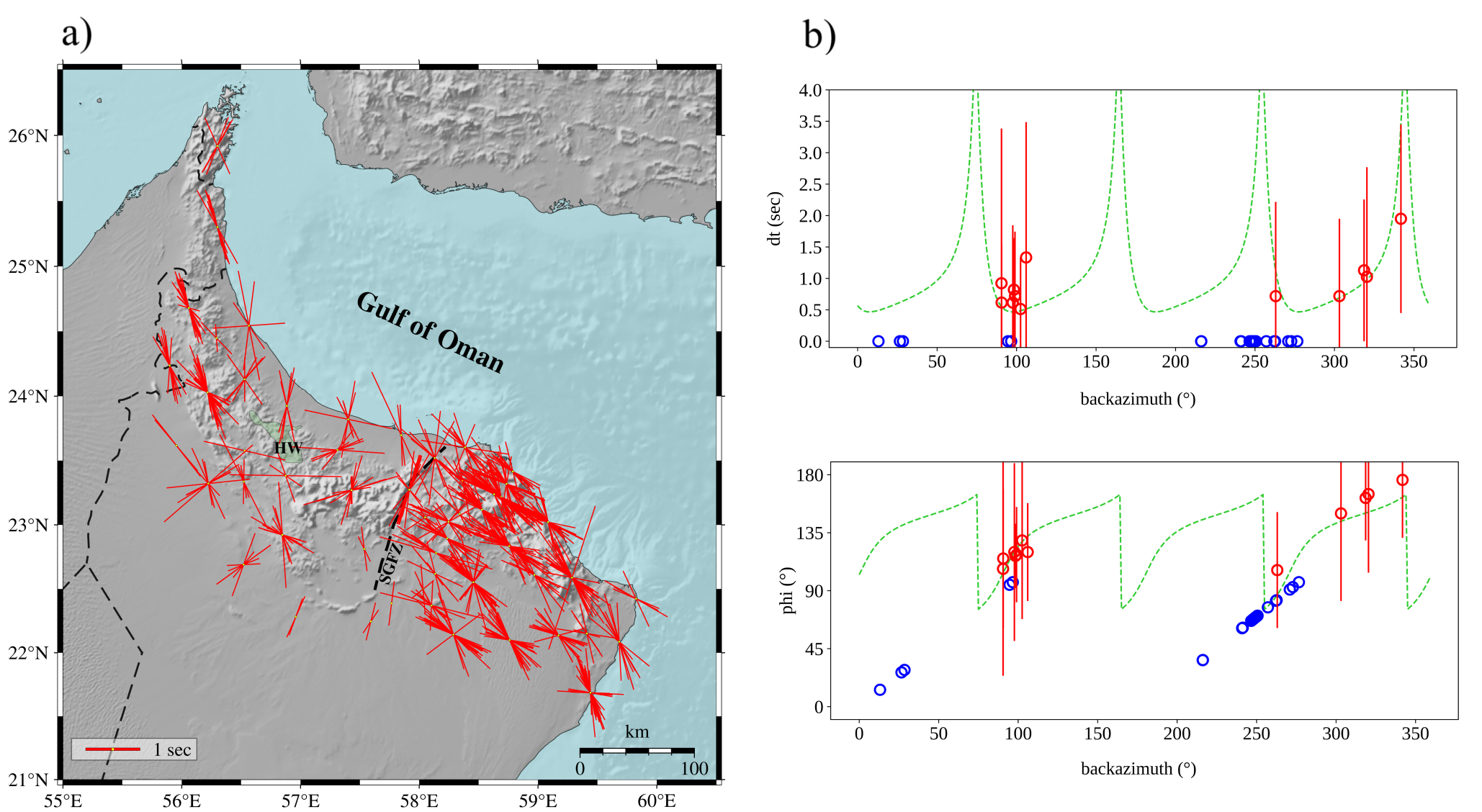
a)
b)
Gulf of Oman
HW
SGFZ
1 sec
km
0
100
26°N
25°N
24°N
23°N
22°N
21°N
55°E
56°E
57°E
58°E
59°E
60°E
dt (sec)
backazimuth (°)
phi (°)
backazimuth (°)

Figure3.

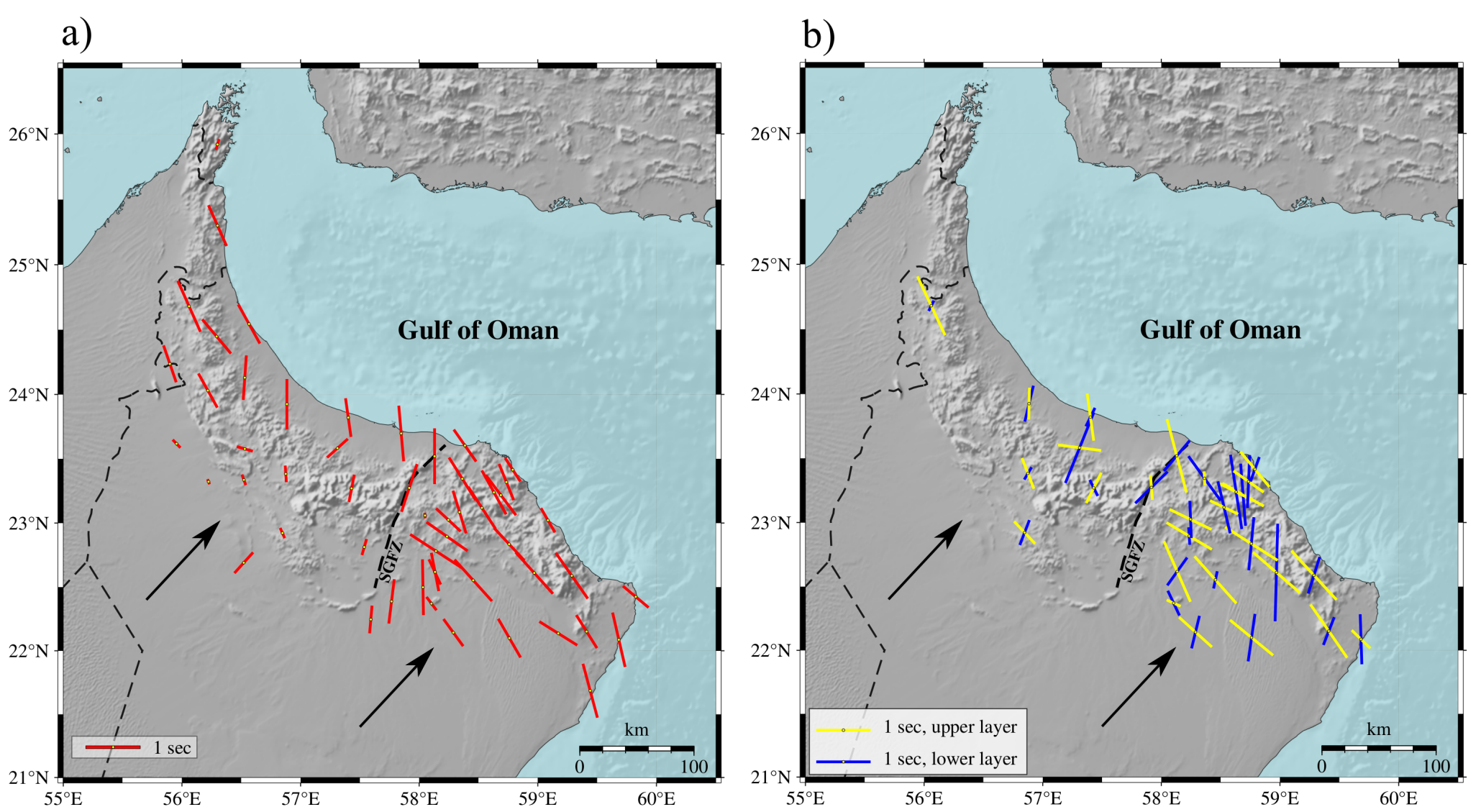
a)
b)
Gulf of Oman
Gulf of Oman
SGFZ
SGFZ
1 sec
1 sec, upper layer
1 sec, lower layer
km
0
100
km
0
100
26°N
25°N
24°N
23°N
22°N
21°N
55°E
56°E
57°E
58°E
59°E
60°E

Figure4.

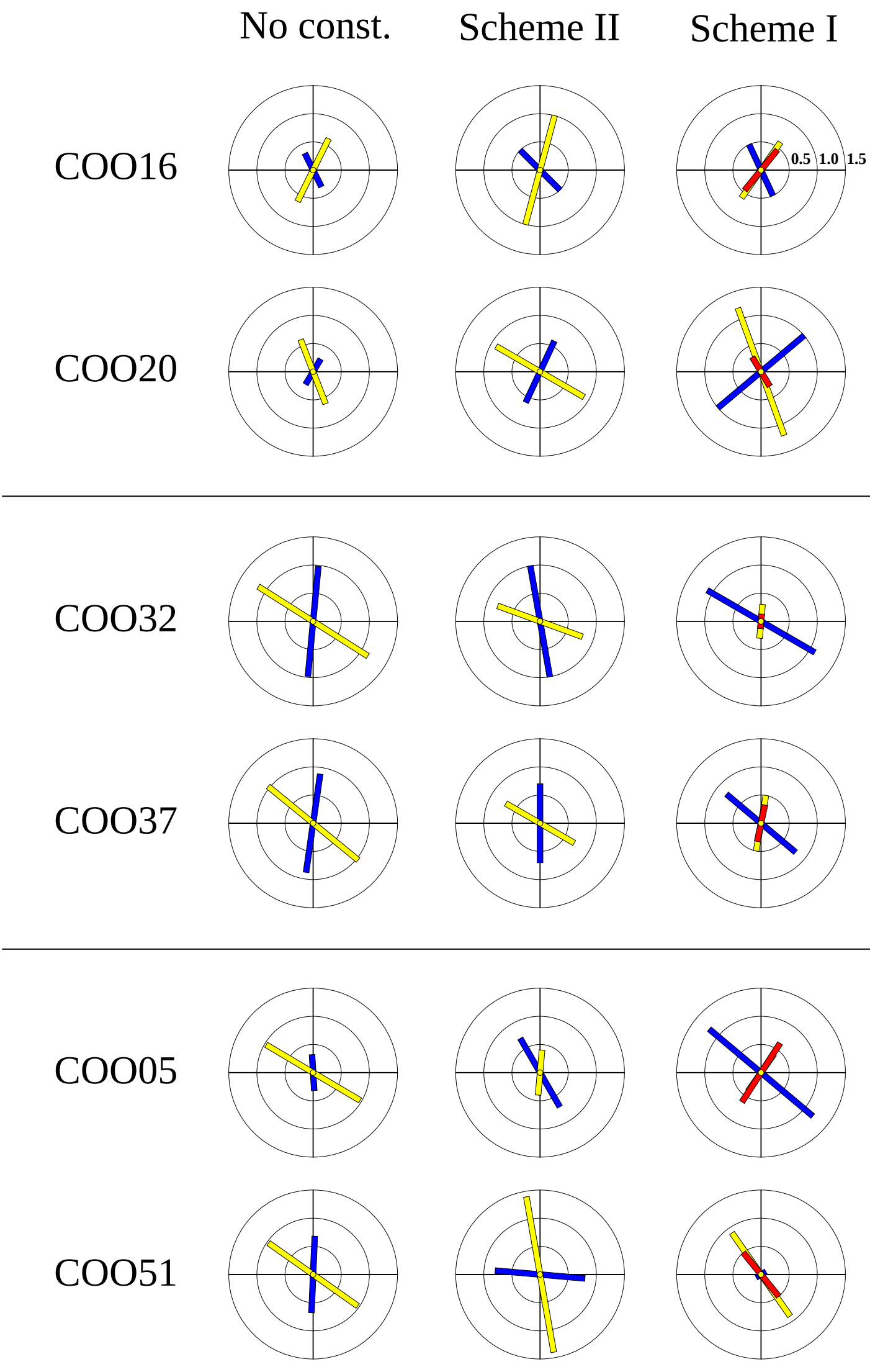
No const.
Scheme II
Scheme I
COO16
COO20
COO32
COO37
COO05
COO51
0.5
1.0
1.5

Figure5.

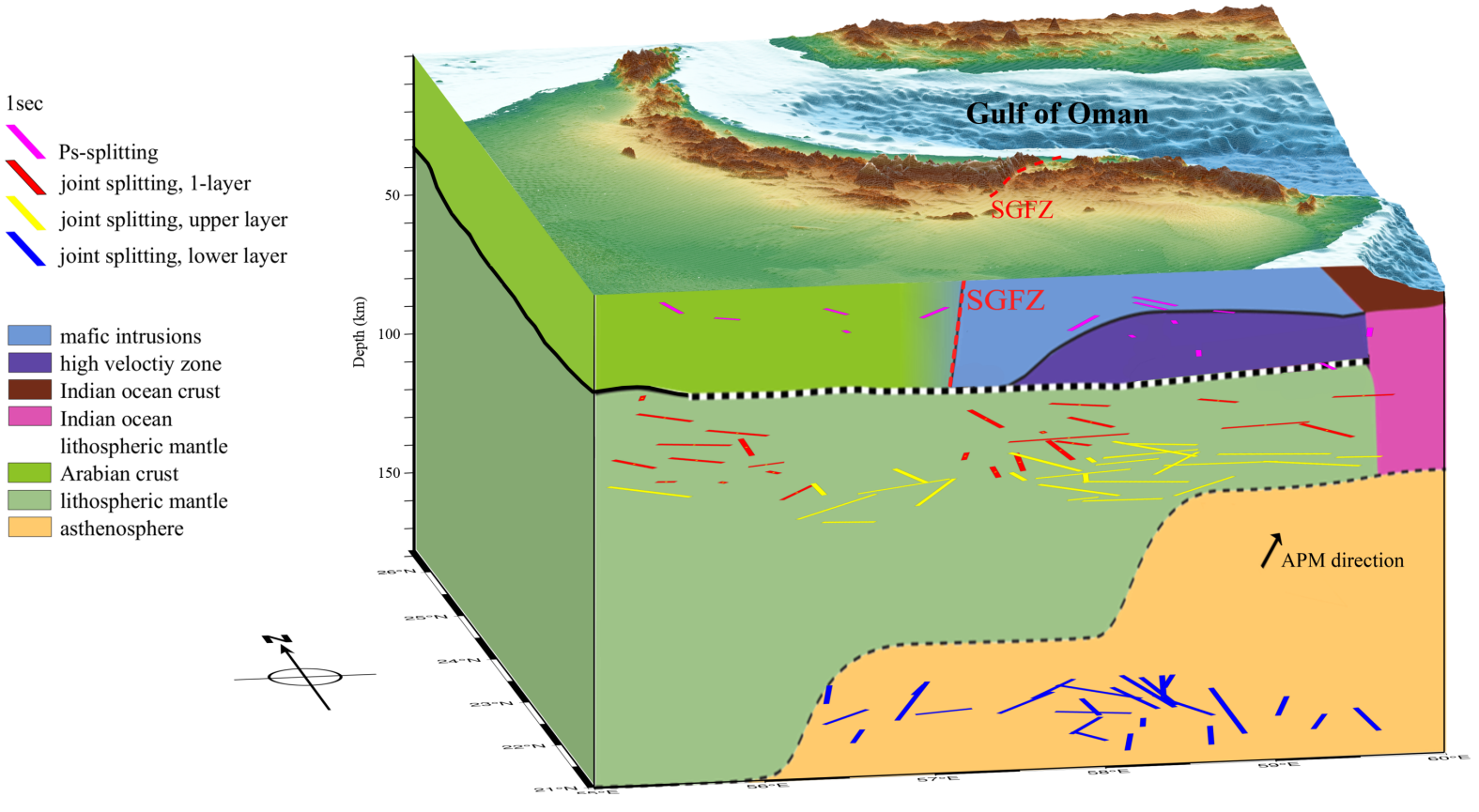
1sec
Ps-splitting
joint splitting, 1-layer
joint splitting, upper layer
joint splitting, lower layer
mafic intrusions
high velocity zone
Indian ocean crust
Indian ocean lithospheric mantle
Arabian crust
lithospheric mantle
asthenosphere
Gulf of Oman
SGFZ
SGFZ
Depth (km)
50
100
150
APM direction
26°N
25°N
24°N
23°N
22°N
21°N
56°E
57°E
58°E
59°E
60°E